X-ray imaging of the interaction between the solar wind and non-magnetized planets

Mats Holmström

IRF Scientific Report 274
March 2001

ISSN 0284-1703

INSTITUTET FÖR RYMDFYSIK

Swedish Institute of Space Physics

Kiruna, Sweden

X-ray imaging of the interaction between the solar wind and non-magnetized planets

BY

MATS HOLMSTRÖM

IRF Scientific Report 274
March 2001

Abstract

Wherever the solar wind meets a neutral atmosphere, X-rays are emitted by charge-exchange processes between heavy solar wind ions and the neutrals. Using an empirical model of the proton flow near Mars we present computer simulations of X-ray emissions from this charge-exchange process in Mars' exosphere. We also predict count rates from this process for observations of Mars and Venus using the X-ray observatories XMM-Newton and Chandra. Finally, we present the discovery of X-ray emissions from Mars by principal component analysis of a 1993 ROSAT observation.

Mats Holmström
Swedish Institute of Space Physics
PO Box 812
SE-98128 Kiruna
Sweden
matsh@irf.se

ISSN 0284-1703

Printed in Sweden by Swedish Institute of Space Physics, Kiruna 2001

Preface

X-rays are generated by charge-exchange wherever the solar wind meets a neutral atmosphere. A highly charged ion in the solar wind captures an electron from a neutral atom or molecule. The ion can be left in an excited state, and when the ion is deexcited, X-rays can be emitted. This is a simple physical process that could have been predicted a long time ago, but interestingly it was not until the emissions were observed (from comets) that this theoretical explanation was suggested. Since the production rate of X-rays by this process is proportional to the ion flux and the neutral density, it is large near non-magnetized planets, where the solar wind comes into direct contact with the lower parts of the planet's exosphere.

The idea behind this report is to collect in one place several aspects of the X-ray emissions from charge-exchange near non-magnetized planets. The report starts with a summary, followed by three papers presenting

1. computer simulations of X-ray emissions near Mars,
2. computer simulations of the count rates from Mars and Venus that would be detected by X-ray imagers in Earth orbit, and
3. the detection of X-rays emitted near Mars in an old (1993) ROSAT observation.

It has been exciting to work on the simulations in this report, since the predicted results are genuinely new and cannot be compared with any existing measurements. Observations will soon be made of Mars and Venus that will prove or disprove the predictions made in this report.

Kiruna, March 9, 2001

Mats Holmström

This report is based on the following papers, which will be referred to in the summary by the Roman numerals [I]-[III].

[I] M. Holmström, S. Barabash and E. Kallio, *X-ray imaging of the solar wind—Mars interaction.* Accepted for publication in *Geophysical Research Letters.*[*]

[II] M. Holmström, *Imaging of the interaction between the solar wind and non-magnetized planets using X-ray observatories.*

[III] L. Liszka and M. Holmström, *X-ray observation of Mars using the ROSAT PSPCB instrument.* Submitted for publication in *Icarus.*

[*] Reprints were made with permission from the publisher.

Summary

In 1996 there was a surprising discovery. The Röntgen X-ray Satellite (ROSAT) observed X-ray emissions from comet Hyakutake [8]. Several mechanisms for the emissions were suggested, but none of them were able to explain the morphology *and* intensity of the emission region. In 1997 it was suggested [2] that the X-ray emissions were due to multiply charged heavy solar wind ions excited by charge-exchange[1] with neutral atoms. Computer simulations [4, 9] have shown that this charge-exchange mechanism is consistent with the ROSAT observations. Proof that this is the correct mechanism came in 2000, when NASA's Chandra X-ray Observatory imaged comet LINEAR and detected X-ray spectral lines from the deexcitation of oxygen and nitrogen ions [7].

X-rays emitted by this charge-exchange mechanism occur not only near comets, but wherever the solar wind meets neutral atoms. The mechanism is as follows. Charge-exchange between a multiply charged ion and a neutral atom can leave the ion in an excited state. When the captured electron then transitions to a lower energy state, within L- and K-shells, X-rays may be emitted. This can occur when heavy ions in the solar wind, such as O^{6+}, C^{6+} and Ne^{8+}, interact directly with a planetary neutral atmosphere. In paper [I] we present the results of computer simulations of the X-ray directional energy flux from charge exchange near Mars. The radiated power at a point is proportional to the heavy ion flux and the neutral density. We compute the neutral density from a standard, spherical symmetric, exospheric model [1]. We used two set of parameters for the neutral model, one that corresponds to a case of high solar activity (solar maximum) and one that corresponds to a case of low solar activity (solar minimum). The heavy ion flux is approximated as a constant fraction of the solar wind proton flux, which is given by an empirical model [5]. The proton flux model is such that the velocity and density are linearly dependent on the solar wind values. Therefore, the emission can increase noticeably, compared to the presented nominal values, when a disturbance of the solar wind hits Mars.

The produced X-rays are emitted uniformly in all directions, and to generate images of the radiated X-rays we let the intensity at each pixel in the image be proportional to the total directional emission along the line-of-sight. The directional intensity is found to be between 100 and 1200 keV/(cm^2 sterad s), depending on solar conditions and view direction. The expected spectrum of the emissions has been predicted by Wegmann et al. [9] and by Kharchenko and Dalgarno [6]. The total power emitted by X-rays inside a sphere of 10 Martian radii, centered at Mars, is between $1.52 \cdot 10^{25}$ eV/s (solar minimum) and $0.93 \cdot 10^{25}$ eV/s (solar maximum). This is consistent with estimates of the total luminosity given by Cravens [3].

We would of course like to validate the predictions from the simulations in paper [I] by observations. At present there are two sensitive X-ray observatories in Earth orbit, NASA's Chandra X-ray Observatory and ESA's XMM-Newton X-ray Observatory. To predict what would be detected by these observatories, we need to convert the directional energy fluxes of paper [I] to count rates. The count rates will depend on the viewpoint of the observer (the position of the Sun, the Earth and Mars) and on instrument specific parameters. In paper [II] we predict the count rates from X-ray emissions near Mars for the X-ray observatories XMM-Newton and Chandra for the years 2001-2004. Observations are constrained by instrument limits on the solar angle. A count rate of at least 20 photons per hour is predicted for XMM-Newton on March 30, 2001 and at least 36 photons per hour on August 27, 2001. On these two dates, Mars can be in XMM's field-of-view for at least 30 and 27 hours, resulting in a predicted total of at least 620 and 970 detected photons.

[1] Charge-exchange is sometimes called charge transfer.

We also predict a count rate of at least 17 photons per hour for Chandra when the Earth-Mars distance is minimal on June 21, 2001.

We also estimate the count rates from Venus for Chandra (it is not possible to observe Venus using XMM-Newton due to solar angle constraints). The emission model for Venus is simply a scaled version of the Mars model. We predict a count rate of at least 170 photons per hour on February 8, 2001 and 130 photons per hour on May 25, 2001. On these two dates, Venus can be in Chandra's field-of-view for at least 15 and 21 hours, resulting in a predicted total of 2,500 and 2,800 detected photons.

Instead of making new observations, an alternative way to validate the predictions from the simulations in paper [I] is to examine old observations. In paper [III] we examine a 1993 ROSAT observation for traces of soft X-ray emissions near Mars. Although the simulations predict too weak emissions to be detected, we present the discovery of soft X-ray emissions from Mars by principal component analysis (PCA).

References

[1] J. W. Chamberlain and D. M. Hunten. *Theory of Planetary Atmospheres.* Academic, San Diego, 2nd edition, 1987. p. 335.

[2] T. E. Cravens. Comet Hyakutake X-ray source: Charge transfer of solar wind heavy ions. *Geophysical Research Letters*, 24(1):105–108, January 1997.

[3] T. E. Cravens. X-ray emissions from comets and planets. *Advances in Space Research*, 26(10):1443–1451, July 24, 2000.

[4] R. M. Häberli, T. I. Gombosi, D. L. De Zeeuw, M. R. Combi, and K. G. Powell. Modeling of cometary X-rays caused by solar wind minor ions. *Science*, 276:939–942, 1997.

[5] E. Kallio and H. Koskinen. A test particle simulation of the motion of oxygen ions and solar wind protons near Mars. *Journal of Geophysical Research*, 104(A1):557–579, January 1999.

[6] V. Kharchenko and A. Dalgarno. Spectra of cometary X rays induced by solar wind ions. *Journal of Geophysical Research*, 105:18,351–18,359, 2000.

[7] C. M. Lisse, D. J. Christian, K. Dennerl, F. E. Marshall, R. Mushotzky, R. Petre, S. Snowden, H. A. Weaver, B. Stroozas, and S. Wolk. Discovery of charge exchange emission from C/LINEAR 1999 S4. Presentation at DPS Pasadena Meeting, October 2000.

[8] C. M. Lisse, K. Dennerl, J. Englhauser, M. Harden, F. E. Marshall, M. J. Mumma, R. Petre, J. P. Pye, M. J. Ricketts, J. Schmitt, J. Trümper, and R. G. West. Discovery of X-ray and extreme ultraviolet emission from comet C/Hyakutake 1996 B2. *Science*, 274:205–209, October 1996.

[9] R. Wegmann, H. U. Schmidt, C. M. Lisse, K. Dennerl, and J. Englhauser. X-rays from comets generated by energetic solar wind particles. *Planetary and Space Science*, 46(5):603–612, 1998.

Paper I

M. Holmström, S. Barabash and E. Kallio
X-ray imaging of the solar wind—Mars interaction
Accepted for publication in *Geophysical Research Letters*

X-ray imaging of the solar wind—Mars interaction

Mats Holmström and Stas Barabash

Swedish Institute of Space Physics, Kiruna, Sweden

Esa Kallio

Finnish Meteorological Institute, Geophysical Research, Helsinki, Finland

Abstract. Wherever the solar wind meets a neutral atmosphere, X-rays are emitted by charge-exchange processes between heavy solar wind ions and the neutrals. Using an empirical model of the proton flow near Mars we present computer simulations of X-ray emissions from this charge-exchange process in Mars' exosphere. We also discuss implications for remote sensing. Here we show that the total X-ray luminosity near Mars from charge-exchange is greater than 10^{25} eV/s for typical solar wind conditions. This flux is large enough to be detected by an X-ray satellite in Earth orbit. Thus, Mars belongs to a new class of X-ray objects in the sky, together with other non-magnetized planets, such as Venus.

Introduction

In 1996 there was a surprising discovery. The Röntgen X-ray Satellite (ROSAT) observed X-ray emissions from comet Hyakutake [*Lisse et al.*, 1996]. Several mechanisms for the emissions were suggested, such as electron bremsstrahlung and scattering of solar X-rays. None of these mechanisms were able to explain the morphology and intensity of the emission region. In 1997 it was suggested [*Cravens*, 1997] that the X-ray emissions were due to multiply charged heavy solar wind ions excited by charge-exchange with neutral atoms. Computer simulations [*Häberli et al.*, 1997; *Wegmann et al.*, 1998] have shown that this charge-exchange mechanism is consistent with the ROSAT observations. Proof that this is the correct mechanism came recently when NASA's Chandra X-ray Observatory imaged comet LINEAR and detected X-rays from oxygen and nitrogen ions [*Lisse et al.*, 2000].

X-rays emitted by this charge-exchange mechanism occur wherever the solar wind meets neutral atoms and in this paper we present the results of computer simulations of X-ray emissions near Mars and implications for remote sensing.

Model

Charge-exchange between a multiply charged ion and a neutral atom can leave the ion in an excited state. When the captured electron then transitions to a lower energy state, within L- and K-shells, X-rays may be emitted. This can occur when heavy ions in the solar wind, such as O^{6+}, C^{6+} and Ne^{8+}, interact directly with a planetary neutral atmosphere, e.g., near Mars.

Paper number 2000GL000000.
0094-8276/01/2000GL000000$05.00

We can estimate the radiated power at a point by

$$p = u_{\rm ion}\, n_{\rm ion}\, n_n\, \sigma\, \Delta E \qquad \left[\mathrm{eV/(cm^3\ s)}\right], \qquad (1)$$

where $u_{\rm ion}$ [cm/s] is the magnitude of the heavy ion velocity, $n_{\rm ion}$ [$\mathrm{cm^{-3}}$] is the ion number density, n_n [$\mathrm{cm^{-3}}$] is the number density of neutral atoms, σ [$\mathrm{cm^2}$] is the cross-section for heavy ion–neutral charge-exchange, and ΔE [eV] is the average emitted energy per heavy ion, that includes the effects of cascading (ions that transition to a lower charge state can transition repeatedly). We regard $u_{\rm ion}$, $n_{\rm ion}$ and n_n as functions of position, while the rest of the parameters are regarded as constants.

The ion velocities and densities are computed from an empirical, axial symmetric proton flow model based on Automatic Space Plasma Experiment with a Rotating Analyzer (ASPERA) ion measurements on the Phobos-2 spacecraft. The model includes three boundaries: the bow shock (BS), the "magnetopause" (MP, subsolar height = $0.2R_m \approx 680$ km), and the ionopause (IP, subsolar height = $0.05R_m \approx 170$ km). Here R_m denotes Mars' radii. In the model the proton flux decrease strongly at the MP while the IP represents an impenetrable obstacle for the flow. Charge-exchange collisions are rare near IP because of the low proton flux downstream of the MP (see, *Kallio et al.*, [1997], Fig. 1d and Fig. 7). A detailed model description can be found in *Kallio and Koskinen*, [1999] and here only certain aspects related to the X-ray emission are considered.

In the empirical model the global electric and magnetic fields can be derived from the velocity model by assuming that the magnetic field is frozen into the flow. The global fields therefore make it possible to study how the ions are accelerated by the Lorentz force near Mars. For example, the solar wind H^+ ion trajectories were found to be described quite well by the flow model for the upstream parameters $u_{\rm sw} = 400$ km/s and $\mathbf{B}_{\rm sw} = (0,\ 2,\ 0)$ nT in *Kallio and Koskinen*, [1999].

The role of kinetic effects for the motion of heavy solar wind ions near Mars can be analyzed similarly by studying the motion of ions near the planet. The magnetic field in the empirical flow model, $\mathbf{B}(\mathbf{r})$, is a product of the magnitude of the magnetic field in the solar wind $B_{\rm sw}$ and the normalized magnetic field vector, $\tilde{\mathbf{B}}(\mathbf{r})$, resulting from the frozen-in condition, $\mathbf{B}(\mathbf{r}) = B_{\rm sw}\tilde{\mathbf{B}}(\mathbf{r})$. The equation of motion for ions relative to the velocity from the empirical model, $\mathbf{U}(\mathbf{r})$, can therefore be expressed as

$$\frac{\mathrm{d}^2\mathbf{r}}{\mathrm{dt}^2} = (\mathbf{v} - \mathbf{U}(\mathbf{r})) \times \tilde{\mathbf{B}}(\mathbf{r}) \qquad \left[B_{\rm sw}(m/q)^{-1}\right], \qquad (2)$$

where $\mathbf{v}$ is the velocity of an ion of mass m and electric charge q.

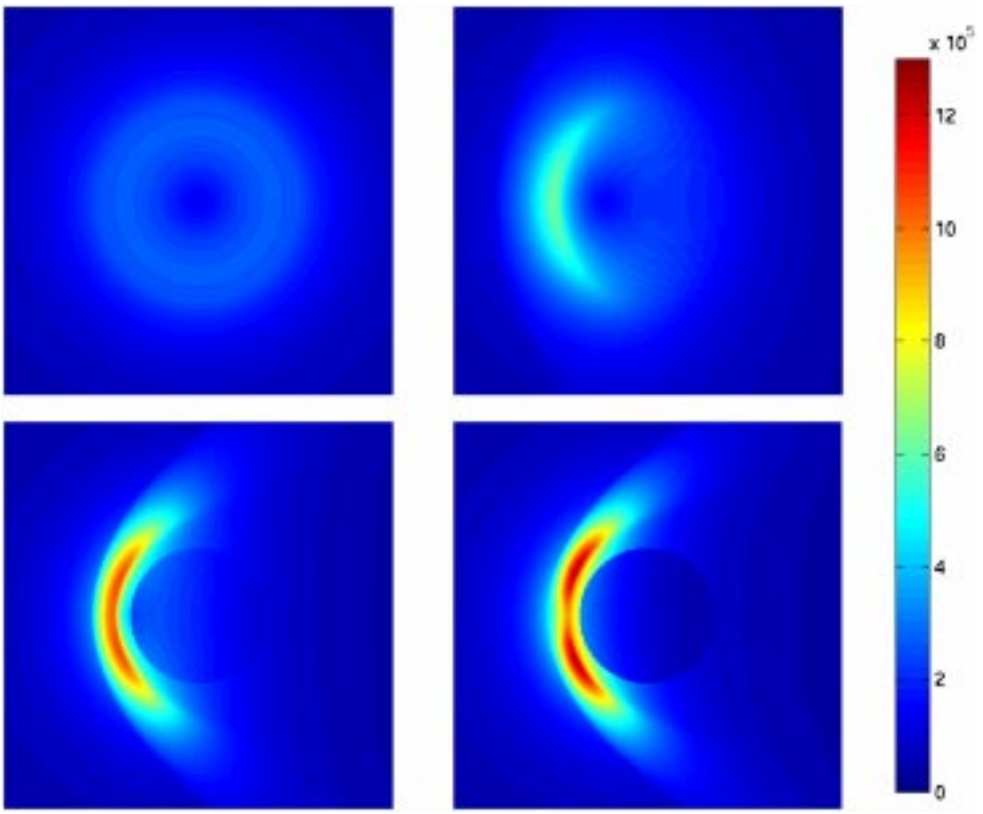

Plate 1. Parallel projections of X-ray emissions near Mars at solar minimum. The angle of the view direction to the Mars—Sun line is, 0 (top left), 30 (top right), 60 (bottom left) and 90 (bottom right) degrees. The intensity is proportional to the directional energy flux [eV/(cm^2 sterad s)]. The extent of the images is $6R_m \times 6R_m$, and they are centered at Mars.

Equation (2) illustrates that in the empirical flow model the gyroradius depends linearly on the magnitude of the IMF and the q/m ratio. If two test particles of different q/m values are launched at the same point, at the same initial velocity, their trajectories will be identical for a given solar wind speed if the runs have the same $B_{\rm sw}(m/q)^{-1}$ value. For example, H^+ ion trajectories presented in *Kallio and Koskinen*, [1999] are identical to the O^{6+} ion ($m/q = 16/6$) trajectories for $\mathbf{B}_{\rm sw}$ = (16/6) (0, 2, 0) nT = (0, 5.33, 0) nT. About 5 nT magnetic field is therefore strong enough to produce a fluid like motion for the heavy O^{6+} ions.

Diminishing IMF enlarges the ion gyroradius, and thereby increases asymmetric flow features that are not included in the used analytical flow model. Fig. 1 shows an example of the motion of O^{6+} ions calculated for $\mathbf{B}_{\rm sw}$ = (0, 4, 0) nT. The trajectories suggest that the used flow model give a relatively good approximation for the motion of heavy ions near Mars at typical IMF conditions. The relative number densities of heavy ions in the solar wind can be found in *Wegmann et al.* [1998] and a mean value for m/q of 2.9 can be computed. Justified by the above discussion, we will approximate the heavy ion velocity in (1) by the proton velocity, $u_{\rm ion} \approx u_p$.

We then approximate the heavy ion number density as a constant fraction, f, of the proton density, $n_{\rm ion} \approx f\, n_p$. In practice, as ions charge-exchange along a stream line, the number of ions in highly charged states will decrease. The radiated power then is

$$p = u_p\, n_p\, n_n\, f\, \sigma\, \Delta E \qquad \left[\mathrm{eV/(cm^3\ s)}\right], \tag{3}$$

where u_p [cm/s] is the magnitude of the proton velocity and n_p [cm^{-3}] is the proton number density.

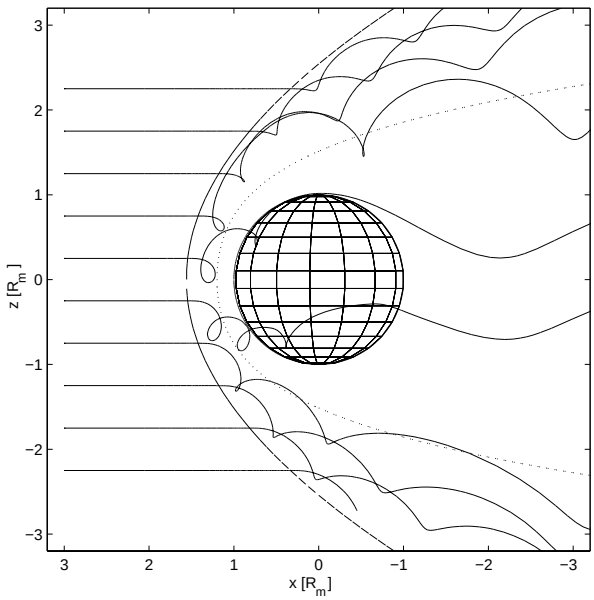

Figure 1. Trajectories for O^{6+} ions ($m/q = 16/6$), when $\mathbf{B}_{\rm sw}$ = (0, 4, 0) nT and $(u_p)_{\rm sw}$ = 400 km/s. This corresponds to trajectories for H^+ ions when $\mathbf{B}_{\rm sw}$ = (6/16)(0, 4, 0) nT.

The proton number density, n_p, is computed from the velocity field using mass conservation. The neutral density, n_n, model includes H, H_2 and O, where thermal and non-thermal oxygen are modeled as two separate species. The atomic and molecular hydrogen models are from *Krasnopolsky and Gladstone*, [1996]. The oxygen model is from *Zhang et al.*, [1993]. Each specie's density, n_i, is modeled as

$$n_i(r) = \alpha_i e^{-\beta_i/r}\zeta(\beta_i/r) \quad \text{and} \quad n_n = \sum_i n_i \quad \left[\text{cm}^{-3}\right],$$

where r is the distance to the planet's center and ζ is Chamberlain's partition function [*Chamberlain and Hunten*, 1987]. From *Kallio et al.*,[1997] we have adopted values of the constants α_i and β_i that corresponds to a case of high solar activity (solar maximum) and a case of low solar activity (solar minimum). Due to a lack of data on the exosphere's composition far from Mars, we have limited the computed X-ray emissions to a sphere of radius 10 R_m centered at Mars. The error introduced is an under-estimation of the emissions.

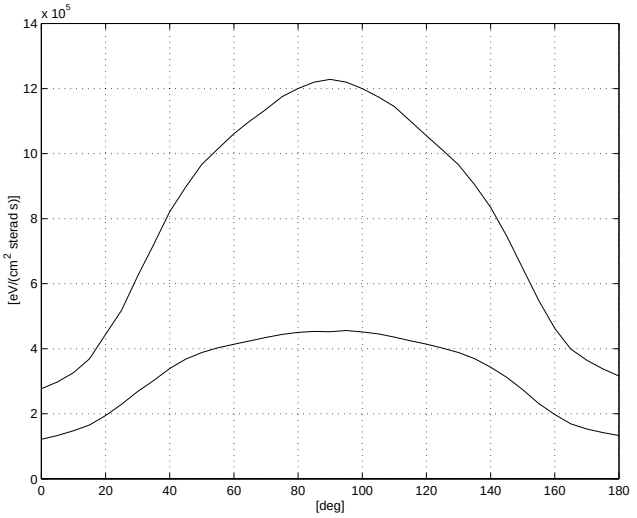

Figure 2. The maximum directional power emitted by X-rays [eV/(cm^2 sterad s)] as a function of the angle [deg] between the view direction and the Mars—Sun line. The upper graph is for a solar minimum atmospheric model and the lower graph for a solar maximum model.

Results

We now compute the total luminosity and generate images of the X-ray radiation near Mars using Equation (3). The values of the parameters used in the simulations are those used by *Wegmann et al.* [1998]; $f = 1.08 \cdot 10^{-3}$, $\sigma = 3 \cdot 10^{-15}\,\text{cm}^2$ and $\Delta E = 205\,\text{eV}$. Where we have computed $\Delta E = 1137\ \text{eV} \cdot 0.4/2.15$ and $f = 2.15 \cdot 5 \cdot 10^{-4}$ from Wegmann's numbers since their parameters are per oxygen ion and our per heavy ion. For the velocity and density model we have used the solar wind values $(u_p)_{\text{sw}} = 400\,\text{km/s}$ and $(n_p)_{\text{sw}} = 2.5\,\text{cm}^{-3}$.

Since the X-rays are emitted uniformly in all directions it follows from (3) that the directional emission is $p/(4\pi)$ [eV/(cm^3 sterad s)]. To generate images of the radiated X-rays we let the intensity at each pixel in the image be proportional to the total directional emission along the line-of-sight. In Plate 1 we show images from four different vantage points for a neutral model that corresponds to low solar activity.

Note that the proton velocity model is such that the velocity and density are linearly dependent on the solar wind values, $(u_p)_{\text{sw}}$ and $(n_p)_{\text{sw}}$. Therefore, the emission can increase noticeably, compared to the presented nominal values, when a disturbance of the solar wind hits Mars because the radiated power also depend linearly on $(u_p)_{\text{sw}}$ and $(n_p)_{\text{sw}}$.

For observations, the emissions directional dependence is of interest. In Fig. 2 we show the maximum directional power emitted by X-rays as a function of the angle between the view direction and the Mars—Sun line for solar minimum and maximum atmospheric models. We see that the directional intensity is between 100 and 1200 keV/(cm^2 sterad s), depending on solar conditions and view direction. This can be compared with the 11 keV/(cm^2 sterad s) background of emissions from solar wind charge-exchange with heliospheric H and He estimated by *Cravens* [2000a]. The directional intensity is large enough to be detected (and imaged) by an X-ray satellite in Earth orbit, such as ESA's XMM-Newton X-ray Space Observatory, or NASA's Chandra X-ray Observatory. The expected spectrum of the emissions is that of *Wegmann et al.* [1998] (their Figs. 3 and 4).

We also compute the total power emitted by X-rays inside the sphere of 10 R_m radius, centered at Mars. At solar minimum this total luminosity is $1.52 \cdot 10^{25}$ eV/s and at solar maximum it is $0.93 \cdot 10^{25}$ eV/s.

Experiments with a non-constant heavy ion fraction, f, along stream lines were performed. This was done by integrating n_{ion} backwards along streamlines to account for ion losses. This resulted in a decrease of the total luminosity by less than 5 %.

We also computed the total X-ray energy flux to Mars' ionopause (subsolar height 0.05 R_m) as 10^{24} eV/s, or 7 % of the total X-ray production, at solar minimum.

Examining the effect of varying the magnetopause position, it was found that the total luminosity changed by less than 20 % when the subsolar height was varied between 0.1 and 0.5 R_m. This can be explained by the fact that although the neutral density is high close to the planet, the flow model's proton flux is small.

Comparing our computed total X-ray luminosity of about 10^{25} eV/s to the estimate for Mars of $6 \cdot 10^{22}$ eV/s given by *Cravens*,[2000b], our luminosity is almost 170 times larger. We see at least two reasons for this. First of all, Cravens estimates the production as $p = 2.5 \cdot 10^{-9} n_n n_p$ [eV/(cm^3 s)], with n_p constant. New estimates [*Cravens*, 2000a; *Kharchenko and Dalgarno*, 2000] of the constant $(2.5 \cdot 10^{-9})$ is at least 10 times larger. The constant we have used, from *Wegmann et al.* [1998], is $2.6 \cdot 10^{-8}$. Secondly, Cravens only uses hot oxygen as the neutral, but in our model both atomic and molecular hydrogen are included. Using only hot and thermal oxygen in our model, we get a total luminosity of $3 \cdot 10^{23}$ eV/s, which is consistent with Cravens' estimate, taking into account the different production constants.

Implications for remote sensing

There is a fundamental difference between emission of X-rays at Mars and at comets. For comets, due to very large spatial scales of the neutral gas distribution, the heavy ion component of the solar wind is totally depleted while moving

through the cometary coma (that is the reason of the absent of the X-ray emission from the tail) and the peak X-ray flux is determined by the heavy ion density [*Dennerl et al.*, 1997]. In contrast, at Mars, the scale of the neutral gas distribution is small in comparison with the charge-exchange distance and a very small fraction of the solar wind ions is lost during the interaction. This fraction amounts to just a few percent and the loss can be disregarded. That means that comets' X-ray emissions can be used to probe the solar wind while at Mars it is a way to probe the planetary environment.

First of all, X-ray imaging of the near-Mars space opens up an exciting opportunities to remotely diagnose the structure of the solar wind interaction region. If we assume that the neutral gas distribution is known, the deconvolution of X-ray images, for example, via forward-modeling, would provide the global distribution of the solar wind heavy ions. This, in turn, can be converted to the proton distribution. Moreover, it would give extra information about the accuracy of the magnetic field model used in this work because the motion of the heavy ions which could be considered as test particles is governed by the Lorentz force. Since X-ray imaging can be performed in the undisturbed solar wind, simultaneous monitoring of the minor ion density and composition is also possible.

Another interesting application would be to monitor, via X-ray emission, the exospheric (hydrogen) distribution at large distances from the planet where resonance scattering Lyman-alpha emission is too faint to be observed by conventional UV instruments.

All the above considerations are applicable for any other non-magnetized planet/satellite with an atmosphere that is directly exposed to the solar wind. For example, Venus and Titan should emit X-rays according to the same mechanism. Venus looks particularly interesting because the change-exchange process is more efficient there [*Russell et al.*, 1983].

References

Chamberlain, J. W., and D. M. Hunten, *Theory of Planetary Atmospheres,* 335 p., Academic, San Diego, Calif., 1987.

Cravens, T. E., Comet Hyakutake X-ray source: Charge transfer of solar wind heavy ions, *Geophys. Res. Lett., 24,* 105-108, 1997.

Cravens, T. E., Heliospheric X-ray emission associated with charge transfer of the solar wind with interstellar neutrals, *Astrophys. J., 532,* L153-L156, 2000a.

Cravens, T. E., X-ray emission from comets and planets, *Adv. Space Res., 26,* 1443-1451, 2000b.

Dennerl, K., J. Englhauser and J. Trümper, X-ray emissions from comets detected in the Röntgen X-ray satellite all-sky survey, *Science, 277,* 1625-1630, 1997.

Häberli, R. M., T. I. Gombosi, D. L. De Zeeuw, M. R. Combi and K. G. Powell, Modeling of cometary X-rays caused by solar wind minor ions, *Science, 276,* 939-942, 1997.

Kallio, E., An empirical model of the solar wind flow around Mars, *J. Geophys. Res., 101,* 11,133-11,147, 1996.

Kallio, E., J. G. Luhmann and S. Barabash, Charge exchange near Mars: The solar wind absorption and energetic neutral atom production, *J. Geophys. Res., 102,* 22,183-22,197, 1997.

Kallio, E. and H. Koskinen, A test particle simulation of the motion of oxygen ions and solar wind protons near Mars, *J. Geophys. Res., 104,* 557-579, 1999.

Kharchenko, V. and A. Dalgarno, Spectra of cometary X rays induced by solar wind ions, *J. Geophys. Res., 105,* 18,351-18,359, 2000.

Krasnopolsky, V. A., and G. R. Gladstone, Helium on Mars: EUVE and PHOBOS data and implications for Mars' evolution, *J. Geophys. Res., 101,* 15,765-15,772, 1996.

Lisse, C. M., K. Dennerl, J. Englhauser, M. Harden, F. E. Marshall, M. J. Mumma, R. Petre, J. P. Pye, M. J. Ricketts, J. Schmitt, J. Trümper and R. G. West, Discovery of X-ray and extreme ultraviolet emission from comet C/Hyakutake 1996 B2, *Science, 274,* 205-209, 1996.

Lisse, C. M., D. J. Christian, K. Dennerl, F. E. Marshall, R. Mushotzky, R. Petre, S. Snowden, H. A. Weaver, B. Stroozas and S. Wolk, Discovery of charge exchange emission from C/LINEAR 1999 S4, paper presented at DPS Pasadena Meeting, October 23 to 27, 2000.

Russell, C. T., T. I. Gombosi, M. Horanyi, T. E. Cravens and A. F. Nagy, Charge-exchange in the magnetosheaths of Venus and Mars: A comparison, *Geophys. Res. Lett., 10,* 163-164, 1983.

Wegmann, R., H. U. Schmidt, C. M. Lisse, K. Dennerl and J. Englhauser, X-rays from comets generated by energetic solar wind particles, *Planet. Space Sci., 46,* 603-612, 1998.

Zhang, M. H. G., J. G. Luhmann, S. W. Bougher, and A. F. Nagy, The ancient oxygen exosphere of Mars: Implications for atmosphere evolution, *J. Geophys. Res., 98,* 10,915-10,923, 1993.

M. Holmström and S. Barabash, Swedish Institute of Space Physics, PO Box 812, SE-98128 Kiruna, Sweden. (e-mail: matsh@irf.se; stas@irf.se)

E. Kallio, Finnish Meteorological Institute, Geophysical Research, PO Box 503, FIN-00101 Helsinki, Finland. (e-mail: Esa.Kallio@fmi.fi)

(Received September 22, 2000; revised December 12, 2000; accepted December 22, 2000.)

Paper II

M. Holmström

Imaging of the interaction between the solar wind and non-magnetized planets using X-ray observatories

Imaging of the interaction between the solar wind and non-magnetized planets using X-ray observatories

Mats Holmström*

January 25, 2001

Abstract

Simulated X-ray images of Mars were presented in a paper by Holmström, Barabash and Kallio [4]. The X-rays are emitted by charge-exchange processes between highly charged solar wind ions and Mars' exosphere. The images show the directional flux of energy in units of [eV/(cm^2 sterad s)]. In order to investigate the possibility of detecting X-rays emitted near Mars by observatories in Earth orbit, we need to predict count rates [counts/s], that will depend on the viewpoint of the observer and on instrument specific parameters. Here we predict count rates for the X-ray observatories XMM-Newton and Chandra as a function of time for the years 2001-2004. XMM-Newton observations are restricted by a maximum allowed solar angle of 110 degrees. A count rate of at least 20 photons per hour is predicted for XMM-Newton on March 30, 2001 and at least 36 photons per hour on August 27, 2001. On these two dates, Mars can be in XMM's field of view for at least 30 and 27 hours, resulting in a predicted total of at least 620 and 970 detected photons. We also predict a count rate of at least 17 photons per hour for Chandra when the Earth-Mars distance is minimal on June 21, 2001.

Since the same charge-exchange processes are present wherever the solar wind meets a neutral atmosphere, we have also estimated the emissions near Venus. For XMM-Newton and Chandra the minimum allowed solar angle is 70 and 45 degrees, respectively. Consequently, it is not possible to observe Venus using XMM-Newton. The solar angle is greater than 45 degrees during six time periods in the years 2001-2004. For Chandra, we predict a count rate of at least 170 photons per hour on February 8, 2001 and 130 photons per hour on May 25, 2001. On these two dates, Venus can be in Chandra's field of view for at least 15 and 21 hours, resulting in a predicted total of 2,500 and 2,800 detected photons.

Introduction

In 1996, X-ray emissions from comet Hyakutake were observed [6], and they were later explained by multiply charged heavy solar wind ions excited by charge-exchange with neutral atoms [2]. X-rays emitted by this charge-exchange mechanism occur wherever the solar wind meets neutral atoms and in a paper by Holmström, Barabash and Kallio [4] simulated X-ray images of the interaction between the solar wind and Mars' exosphere were presented.

These simulated images show the directional flux of energy emitted near Mars. To predict what would be detected by observatories in Earth orbit, we need to

*matsh@irf.se, Swedish Institute of Space Physics, PO Box 812, SE-98128 Kiruna, Sweden

predict count rates that will depend on the viewpoint of the observer (the position of the Sun, the Earth and Mars) and on instrument specific parameters. In this paper we predict the count rates from X-ray emissions near Mars for the X-ray observatories XMM-Newton and Chandra. We also estimate the count rates from Venus for Chandra.

Since significant X-ray emissions from Mars and Venus have not been detected before (as far as the author know), discovery of such emissions would identify a new class of X-ray objects in the sky, non-magnetized planets. It would also provide a unique new method to study the solar wind—planetary interaction using remote, rather than in situ observations.

Theory

We start with the simulated X-ray images from [4]. They are generated by line-of-sight integration of the directional X-ray emissions near Mars, which in turn are computed using a proton flow model and a neutral model. The images are parallel projections and they show the directional flux of energy, a two-dimensional function, $p(x, y)$ [eV/(cm^2 sterad s)]. A parallel projection corresponds to an observer at an infinite distance and has the advantage of providing a good approximation to the image observed from any viewpoint, as long as the viewing distance is much larger than the image extent. In particular, this is true when observing Mars from Earth. We only consider photons of energy greater than 50 eV. The position, (x, y), is given in a coordinate system centered at Mars with the x- and y-axis perpendicular to the view direction. The length unit is R_m, Mars radius. The view direction is at an angle α to the Mars-Sun direction. Since the X-ray emissions are symmetric around the Mars-Sun axis, α parametrizes all possible view directions. The symmetry of the X-ray emissions results from the proton flow model being cylindrical symmetric around the Mars-Sun axis, and the neutral model being spherical symmetric around the center of Mars. Thus, for a given flow and neutral model, a parallel projected image from any direction is given by the one-parameter family of images $p_\alpha(x, y)$, where $0 \leq \alpha \leq 180$ degrees. For example, $\alpha = 0$ corresponds to a view from the Sun toward Mars. Images for $\alpha = 0$, 30, 60 and 90 degrees are shown in Figure 1.

Now we want to predict the count rate if we, using an X-ray imager, observe a region of such a simulated image. Denote the area of the observed region by A [(AU)^2]. The solid angle subtended by A, from a certain viewpoint, we denote by $\Omega = A/r^2$ [sterad], where r [AU] is the distance from the viewpoint to the emissions. We assume that $\Omega \ll 1$ ($A \ll r^2$) and that the depth of the emission volume is much smaller than r. This justifies our use of images that are parallel projections in what follows, instead of viewpoint specific images. The total energy flux registered by an X-ray imager is

$$E = \bar{p}\,\Omega\, a \qquad [\text{eV/s}], \tag{1}$$

where a is the effective area of the imager and $\bar{p}$ is the average directional energy flux from A,

$$\bar{p} = \frac{1}{A}\int_A p_\alpha(x, y)\, dA \qquad [\text{eV/(cm}^2 \text{ sterad s)}]. \tag{2}$$

The geometry and notation is illustrated in Figure 2.

Since the imager's effective area is energy dependent ($a = a(E_p)$, where E_p is the photon energy) we should use the differential directional energy flux, $p_\alpha(x, y, E_p)$ in (1-2) and then integrate over energy, $\int p_\alpha(x, y, E_p)\, a(E_p)\, dE_p$, but to simplify we have used a constant a. We choose a at the average photon energy, $\bar{E}$, for the emissions. The spectrum of the emissions is a line spectrum [5], but can be approximated by a continuous bremsstrahlung spectrum with $kT = 230$ eV [10]. Since the

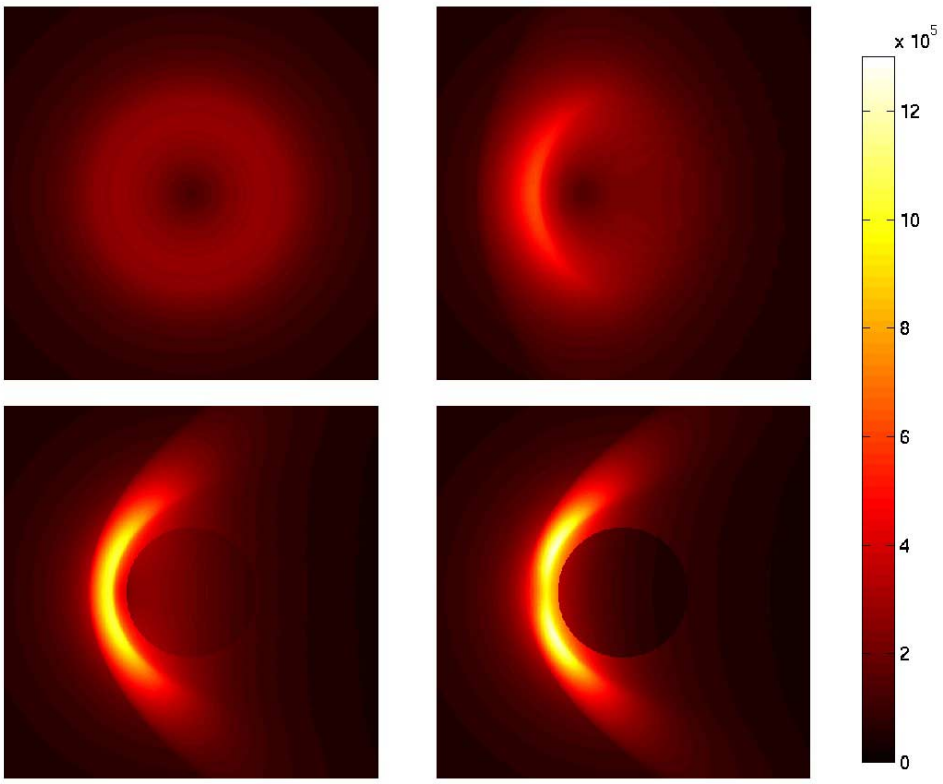

Figure 1: Parallel projections of X-ray emissions near Mars at solar minimum. The angle of the view direction to the Mars—Sun line is, 0 (top left), 30 (top right), 60 (bottom left) and 90 (bottom right) degrees. The intensity is proportional to the directional energy flux [eV/(cm^2 sterad s)]. The extent of the images is $6R_m \times 6R_m$, and they are centered at Mars.

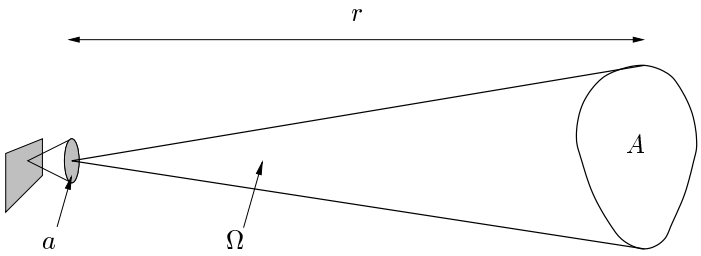

Figure 2: The imager's effective area is a. The solid angle Ω corresponds to an emission region of area A at a distance r from the imager.

Table 1: Average directional flux, $\bar{p}$ [keV/(cm^2 sterad s)], as a function of the Sun-Mars-Earth angle, α [deg], for solar minimum and maximum atmospheric conditions. Computed using (2) for the images in Figure 1.

α	0	30	60	90
$\bar{p}_{\min}$	141	149	152	147
$\bar{p}_{\max}$	74	79	81	79

simulations only consider photons with energy larger than 50 eV, an average photon energy of $\bar{E} = 280$ eV is used. With this average photon energy we can convert (1) to a count rate,

$$P = \bar{p}\,\Omega\, a/\bar{E} \qquad [\text{counts/s}], \tag{3}$$

where a is the effective area at 280 eV and $\Omega = A/r^2$.

The same charge-exchange process occurs at Venus. The simulation results for Mars cannot directly be applied to Venus due to its different exosphere and solar wind flow, but the higher solar wind flux and greater neutral scale height of Venus should make the emissions even greater than for Mars [9].

Let us try to do a rough estimate of the emissions from Venus, using the existing Mars images. Assuming that the proton flow around the non-magnetized planets Mars and Venus has the same morphology, we need to account for the following three differences.

1. The solar wind proton flux is higher at Venus than at Mars. Since the flux decreases as $1/r^2$, where r is the sun distance, we need to scale the count rate by a factor $(r_m/r_v)^2 \approx (1.5/0.75)^2 = 4$, where r_m and r_v are the Sun-Mars and Sun-Venus distances.

2. We need to use Venus' radius, R_v, instead of Mars' radius, R_m. This changes the area of the emission region, A, by a factor of $(R_v/R_m)^2 \approx 3.3$.

3. Different scale height and exobase density for Mars and Venus. We do not account for this, except for the radius scaling in the previous item.

The count rate when observing Venus is then estimated as

$$P_v = \beta P, \tag{4}$$

with $\beta \approx 13$ from item 1 and 2 above. Here P is the corresponding count rate for Mars from (3).

Results

In the first subsection we present count rate estimates for Mars observations as a function of time for the years 2001-2004 using XMM-Newton and Chandra. In the second subsection we present the same information for Venus using only Chandra, since XMM's minimum solar angle of 70 degrees precludes Mars observations.

As in Figure 1 we choose a $6R_m \times 6R_m$ square, centered at Mars, as our emission region, with area $A = 1.74 \cdot 10^{-8}$ [(AU)^2]. In what follows, we use two atmospheric models. A solar maximum and a solar minimum model [4]. We start by computing the average directional flux, $\bar{p}$, by averaging the images in Figure 1 according to (2) and show the dependence on the Sun-Mars-Earth angle, α, in Table 1. This angular dependence is due to shading by Mars. We see that the change in $\bar{p}$ is less than 10% when $0 \leq \alpha \leq 90$ degrees. We also note that $\bar{p}$ is minimal at opposition ($\alpha = 0$)

Table 2: Estimates of different imagers' parameters. From each instruments' on-line documentation [8, 12, 1].

Observatory	Effective area at 280 eV a [cm^2]	Mirror resolution [arcsec]	Pixels per R_m at 0.5 AU
ROSAT (PSPCB)	42	15	0.6
XMM-Newton (EPIC)	1000	6	1.5
Chandra (ACIS-S)	210	0.5	18

and we will use those values ($\bar{p}_{\min} = 141$ and $\bar{p}_{\max} = 74$) in the computations that follows.

We need an estimate of the imagers' effective areas, a, at 280 eV. In Table 2 we show a and also the angular resolution (from which pixels per R_m at 0.5 AU can be calculated) for ROSAT, XMM-Newton and Chandra [8, 12, 1].

Using the Earth-planet distances shown in Figure 3 for the years 2001-2004 we can compute the solid angle, Ω, corresponding to an observation of the $6R_m \times 6R_m$ square from Earth as a function of time. Planet positions were computed using Xephem [11].

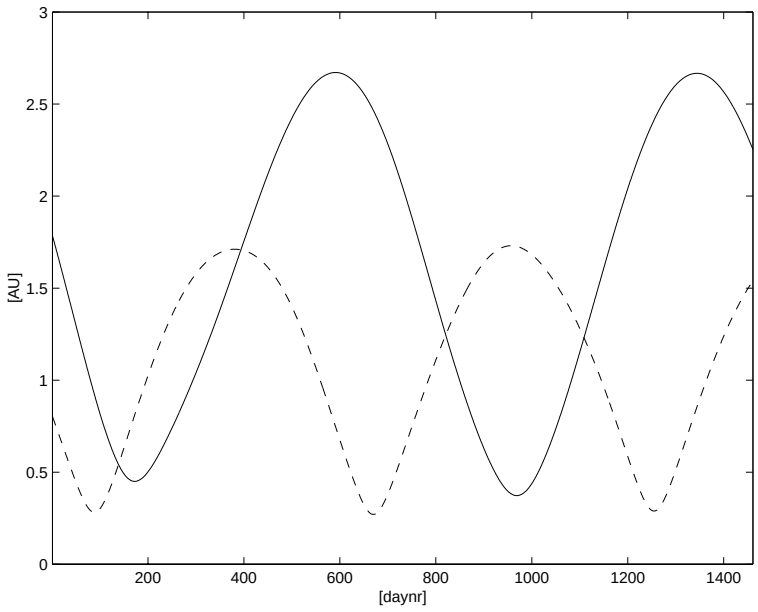

Figure 3: The Earth-Mars (solid line) and Earth-Venus (dashed line) distance [AU] as a function of time [daynr] from 2001-01-01 to 2004-12-31.

An observational restriction is the instruments' allowed solar angles (Sun-planet angular separation). For XMM-Newton and Chandra the minimum allowed solar angle is 70 and 45 degrees, respectively. For XMM-Newton there is also a maximum allowed solar angle of 110 degrees.[1] In Figure 4 we show the solar angle of Mars and Venus as a function of time, along with the limits for XMM-Newton and Chandra. We see that Chandra can observe Mars during opposition, while XMM-Newton only can observe Mars in time periods before and after opposition. The proximity of

[1] I thank Dr. K. Dennerl, Max-Planck-Institut für extraterrestrische Physik, Garching, for pointing out to me XMM's 110 degree maximum solar angle limit.

Venus to the Sun is an observational problem. The maximum angular separation of Venus and the Sun is around 47 degrees. Consequently, it is not possible to observe Venus using XMM-Newton and Chandra can only make observations during short time periods.

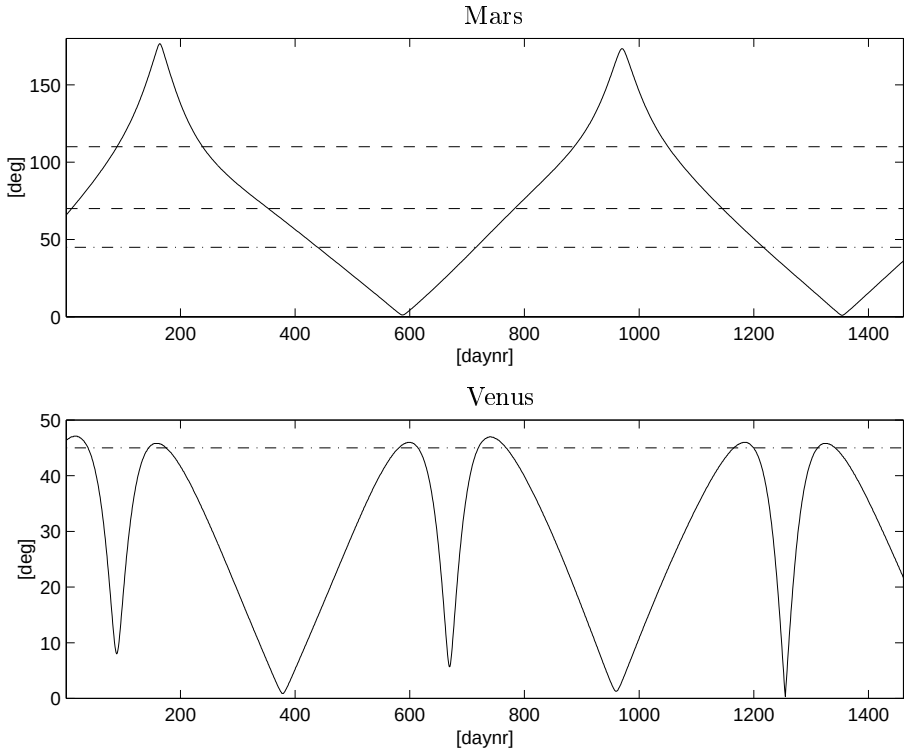

Figure 4: The solar angle (angular separation from the Sun) [deg], for Mars (upper graph) and Venus (lower graph), as a function of time [daynr] from 2001-01-01 to 2004-12-31. The dashed lines show the allowed solar angles for XMM-Newton (between 70 and 110 degrees) and the dashed-dotted lines the minimum solar angle for Chandra (45 degrees).

Mars

We use (3) to predict count rates as a function of time for Mars observations, and they are shown in Figure 5 for Chandra and XMM-Newton. Allowed solar angles are marked in the graphs. The maximum count rate for Chandra occurs when the Earth-Mars distance is minimal, and for XMM-Newton when the solar angle is the maximum allowed (110 degrees). All the local maxima of the count rate are shown in Table 3.

As an illustration, we show in Figure 6 what the spatial distribution of 1000 detected photons could look like. The simulation was done by distributing photons with a probability proportional to the directional emission, $p(x, y)$, at opposition. It is possible to discern the torus shaped region of emissions in front of Mars, as seen in Figure 1. We also show in Figure 7 the spatial distribution of 1000 photons at opposition, binned according to the XMM-Newton pixel size at 0.5 AU (Table 2).

Since XMM-Newton cannot track solar system objects, an observation must be made with the telescope pointing in a fix direction in the equatorial frame of reference. This means that the maximum observation time for Mars is limited by the

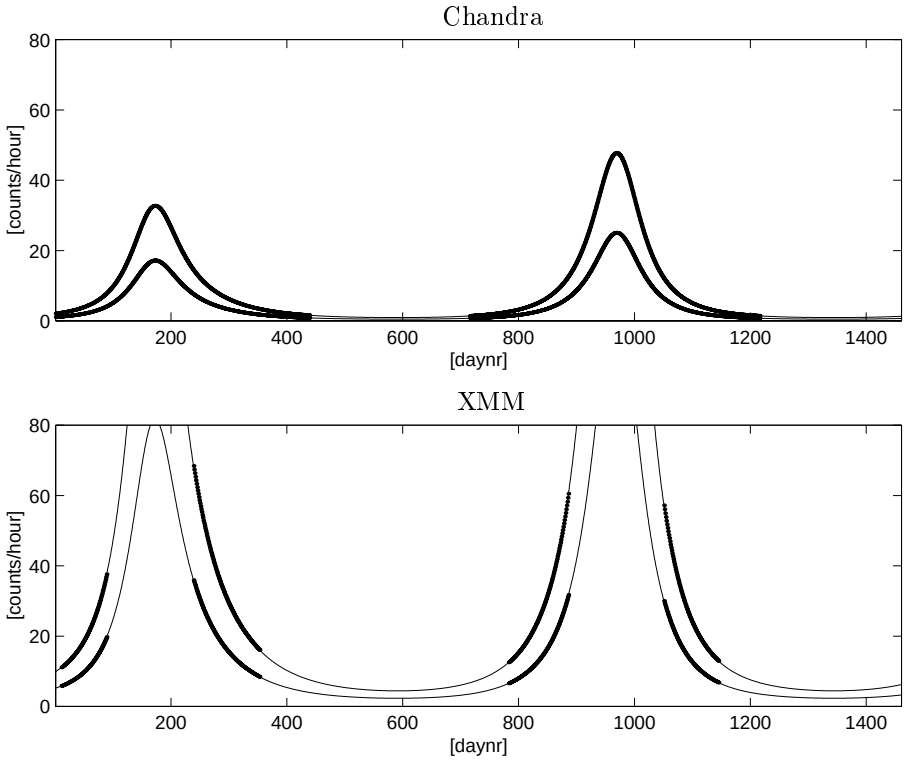

Figure 5: Predicted count rates [counts/hour] when observing Mars using, Chandra (upper graph) and XMM-Newton (lower graph), as a function of time [daynr] from 2001-01-01 to 2004-12-31. The upper curve, in each graph, is for a solar minimum atmospheric model, and the lower for a solar maximum model. Count rate values corresponding to dates when an observation would be possible (considering the instruments' solar angle limits) are marked by dots.

Table 3: Local maxima of the count rate shown in Figure 5 for observing Mars using Chandra and XMM-Newton. The two count rates are for a solar maximum and a solar minimum atmospheric model.

Observatory	Date	Count Rate [counts/hour]	Earth-Mars distance [AU]
Chandra	21-Jun-2001	17-33	0.450
	27-Aug-2003	25-48	0.373
XMM-Newton	30-Mar-2001	20-38	0.916
	27-Aug-2001	36-68	0.679
	05-Jun-2003	32-60	0.723
	17-Nov-2003	30-57	0.743

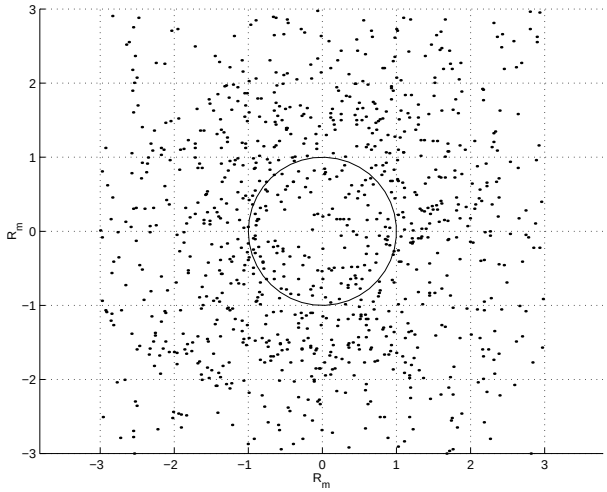

Figure 6: Simulation of the spatial distribution of 1000 photons at opposition. Each dot corresponds to the location of a detected photon. The circle shows the position of Mars.

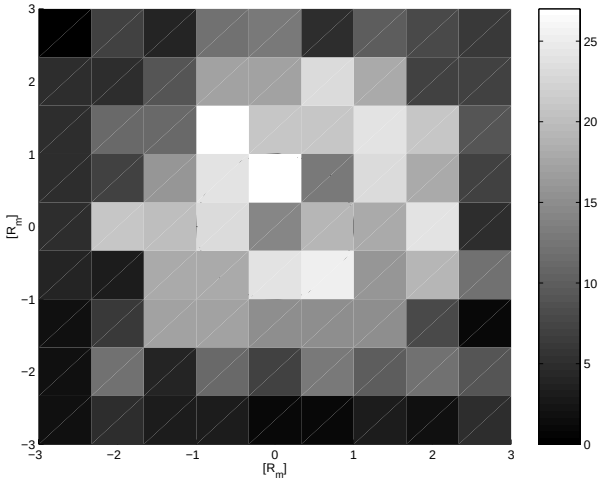

Figure 7: Simulation of the number of counts per pixel for 1000 detected photons at opposition. This is the spatial distribution of photons from Figure 6, binned according to the XMM-Newton pixel size at 0.5 AU. The instrument's point spread function was not accounted for.

time it takes Mars to drift across XMM's field of view. In Figure 8 we show Mars' angular velocity in the equatorial frame as a function of time. For Mars 30 and Au-

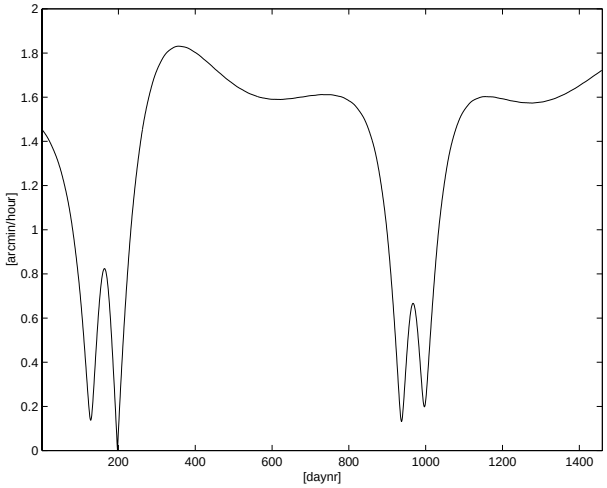

Figure 8: The angular velocity [arcmin/hour] of Mars in the equatorial frame as a function of time [daynr] from 2001-01-01 to 2004-12-31.

gust 27, 2001 (the dates with maximum count rates that year) the velocities are 0.94 and 1.08 arcmin/hour. Since XMM's field of view is 30 arcmin, we get a maximum observational times of 31 and 27 hours. For an m hour observation we can simply point XMM in the direction where the center of Mars will be in $m/2$ hours. Using the count rates of 20-38 and 36-68 counts/hour (from Table 3) results in a predicted total of 620-1,200 and 970-1,800 detected photons, respectively.

Finally, we computed a count rate of 0.4-0.8 counts/hour for a 1993 ROSAT observation ($\alpha = 90$ deg and an Earth-Mars distance of 1.3 AU). This is an order of magnitude smaller than estimates (using principal component analysis of the ROSAT images) by Liszka and Holmström [7]. This can be a random deviation due to the low number of detected photons. Another possible explanations is the detection of photons emitted from outside the $6R_m \times 6R_m$ box. See the section Uncertainties for additional explanations.

Venus

As mentioned before, XMM-Newton cannot observe Venus due to its proximity to the Sun, and Chandra can only make observations during six short time periods in the years 2001-2004 when Venus solar angle is greater than 45 degrees, as shown in Figure 4. The maximum count rate occur either at the start of, or at the end of, each time period. The time periods along with count rates and the predicted total numbers of detected photons are shown in Table 4.

Uncertainties

Some of the uncertainties in the above described count rate predictions are as follows.

1. The solar wind proton flux can be much larger than the values used in our simulations (a velocity of 400 km/s and a number density of 2.5 cm^{-3}) [4]. The model is such that the count rate increases linearly with the flux.

Table 4: Predicted count rates when observing Venus using Chandra. Listed is the start- and end-dates' count rates for the six time periods when Venus' solar angle is greater than 45 degrees, as shown in Figure 4. The date of each time period's maximum count rate (always at the start or end of a time period) is shown in bold face. The two count rates are for a solar maximum and a solar minimum atmospheric model. We also show Venus' angular velocity at maximum count rate dates, along with maximum observation time given Chandra's 30 arcmin field of view. From this we have computed predicted total number of detected photons.

Date	Count Rate [counts/hour]	Earth-Venus distance [AU]	Venus' vel. [arcmin/hour]	max. obs. [hours]	total nr. of counts
08-Feb-2001	166-315	0.523	2.0	15	2,500-4,700
25-May-2001	129-246	0.592	1.4	21	2,800-5,300
24-Jun-2001	65-125	0.832			
04-Aug-2002	66-126	0.827			
06-Sep-2002	141-269	0.566	2.1	14	2,000-3,800
21-Dec-2002	168-320	0.519	2.0	15	2,500-4,500
07-Feb-2003	58-111	0.881			
10-Mar-2004	62-118	0.855			
14-Apr-2004	132-251	0.586	2.1	14	1,900-3,600
03-Aug-2004	127-242	0.596	2.1	14	1,800-3,500
03-Sep-2004	65-123	0.837			

2. We have not taken in to account all the details of the charge exchange process since we have used an average photon energy. A more detailed analysis would take into account the discrete spectrum [5]. Also, Kharchenko [5], show that a value of $kT = 700$ eV might be a better fit to the spectrum than the value of 230 eV used here. The effect of a larger value of $\bar{E}$ would, at least in part, be offset by a large effective area, a in (3).

3. Emissions from charge-exchange processes below 50 eV will be detected above 50 eV, and vice versa, due to the instruments' finite energy resolution. This affects the detected count rate.

4. The background from interplanetary H and He charge-exchange is 11 keV/(cm^2 sterad s) and the total background measured by ROSAT is about twice as large [3]. That is well below our averages of 74-171 for Mars (Table 1).

5. We have not accounted for emissions from outside the $6R_m \times 6R_m$ square.

6. We have used a constant effective area, a, at the average photon energy, 280 eV. The effective area is energy dependent and increasing at this energy for XMM-Newton and Chandra. There is also a sharp drop at 284.5 eV for all three instruments, most pronounced for ROSAT [8]. This is the binding energy of the inner electrons of carbon.

Conclusions

The most favorable time to observe X-rays generated by charge-exchange near Mars depends on the relative positions of the Sun, the Earth and Mars and on the instrument used for the observation. The predicted count rate will also depend on the atmospheric model and emission region used in the simulations. For XMM-Newton, there are two local maxima of the predicted count rate in the year 2001.

On March 30, 20-38 photons per hour, and on August 27, 36-68 photons per hour. The longest possible observational time on these dates give a predicted total of 620-1,200 and 970-1,800 detected photons. For Chandra, we predict a count rate of 17-33 photons per hour on June 21, 2001. For observations of Venus using Chandra the most favorable times in 2001 are on February 8 and May 25 with count rates of 170-310 and 130-250 photons per hour. The longest possible observational time on these dates give a predicted total of 2,500-4,700 and 2,800-5,300 detected photons.

References

[1] The Chandra Proposers' Observatory Guide. Version 3.0. Harvard-Smithsonian Center for Astrophysic, Chandra X-ray Center, Cambridge, Massachusetts, December 28, 2000. `http://asc.harvard.edu/udocs/docs/POG/MPOG/`.

[2] T. E. Cravens. Comet Hyakutake X-ray source: Charge transfer of solar wind heavy ions. *Geophysical Research Letters*, 24(1):105–108, January 1997.

[3] T. E. Cravens. Heliospheric X-ray emission associated with charge transfer of the solar wind with interstellar neutrals. *The Astrophysical Journal*, 532:L153–L156, 2000.

[4] M. Holmström, S. Barabash, and E. Kallio. X-ray imaging of the solar wind—Mars interaction. Accepted for publication in *Geophysical Research Letters*, December 2000.

[5] V. Kharchenko and A. Dalgarno. Spectra of cometary X rays induced by solar wind ions. *Journal of Geophysical Research*, 105:18,351–18,359, 2000.

[6] C. M. Lisse, K. Dennerl, J. Englhauser, M. Harden, F. E. Marshall, M. J. Mumma, R. Petre, J. P. Pye, M. J. Ricketts, J. Schmitt, J. Trümper, and R. G. West. Discovery of X-ray and extreme ultraviolet emission from comet C/Hyakutake 1996 B2. *Science*, 274:205–209, October 1996.

[7] L. Liszka and M. Holmström. X-ray observation of Mars using the ROSAT PSPCB instrument. Submitted for publication in *Icarus*.

[8] ROSAT User's Handbook. Max-Planck-Institut für extraterrestrische Physik, Garching, December 1996. `http://wave.xray.mpe.mpg.de/rosat/doc/ruh/`.

[9] C. T. Russell, T. I. Gombosi, M. Horanyi, T. E. Cravens, and A. F. Nagy. Charge-exchange in the magnetosheaths of Venus and Mars: A comparison. *Geophysical Research Letters*, 10:163–164, 1983.

[10] R. Wegmann, H. U. Schmidt, C. M. Lisse, K. Dennerl, and J. Englhauser. X-rays from comets generated by energetic solar wind particles. *Planetary and Space Science*, 46:603–612, 1998.

[11] Xephem 3.0 by E. C. Downey, February 1997, `http://www.clearskyinstitute.com/xephem/xephem.html`.

[12] The XMM Users' Handbook, Version 1.2, European Space Agency, XMM-Newton Science Operations Centre, March 31, 2000. `http://xmm.vilspa.esa.es/user/uhb_top.html`.

Paper III

L. Liszka and M. Holmström
X-ray observation of Mars using the ROSAT PSPCB instrument
Submitted for publication in *Icarus*

X-ray observation of Mars using the ROSAT PSPCB instrument

Ludwik Liszka* Mats Holmström†

February 23, 2001

Abstract

Here we present the discovery of soft X-ray emissions from Mars by principal component analysis of a 1993 ROSAT observation. The X-rays are probably produced by multiply charged heavy solar wind ions, excited by charge-exchange with neutral atoms in Mars' exosphere, but the detected number of photons is larger than what is predicted by computer simulations.

1 Introduction

In 1996, X-ray emissions from comet Hyakutake were observed (Lisse *et al.* 1996), and they were later explained by multiply charged heavy solar wind ions excited by charge-exchange with neutral atoms (Cravens 1997). X-rays emitted by this charge-exchange mechanism occur wherever the solar wind meets neutral atoms. The mechanism is as follows. Charge-exchange between a multiply charged ion and a neutral atom can leave the ion in an excited state. When the captured electron then transitions to a lower energy state, within L- and K-shells, X-rays may be emitted. This can occur when heavy ions in the solar wind, such as O^{6+}, C^{6+} and Ne^{8+}, interact directly with a planetary neutral atmosphere.

In this paper, we study a 1993 ROSAT observation. First we estimate expected count rates by computer simulations. Then we analyze the observed images using principal component analysis.

2 Simulations

Here we will predict the expected soft X-ray count rate for the 1993 ROSAT observation analyzed later in this paper. We use the simulated X-ray images of the interaction between the solar wind and Mars' exosphere presented in a paper by Holmström *et al.* (2001). The images are generated by line-of-sight integration of the directional X-ray emissions near Mars, which in turn are computed using a proton flow model, and a neutral model. The images are parallel projections, corresponding to an observer at infinite distance. The extent of the images are 6×6 Mars' radii. They show the directional flux of energy in eV/(cm^2 sterad s). We can estimate the count rate for the ROSAT observation as

$$P = \frac{\bar{p}\, A\, a}{r^2\, \bar{E}} \qquad \text{[counts/s]}, \tag{1}$$

where $\bar{p}$ is the average directional energy flux for a simulated image, A is the area of the image, r is the Earth-Mars distance and a is ROSAT's effective area at the average emitted photon energy, $\bar{E}$. From the simulations (Holmström *et al.* 2001) we have the value $\bar{p} = 74$ eV/(cm^2 sterad s). For this observation the Earth-Mars distance $r = 1.3$ AU. We used the values $a = 42$ cm^2 and $\bar{E} = 280$ eV. From Eq. 1, we predict a count rate of 0.4-0.8 counts/hour.

*ludwik@irf.se, Swedish Institute of Space Physics, Umeå Division, Sörfors 634, SE-90588 Umeå, Sweden.
†matsh@irf.se, Swedish Institute of Space Physics, PO Box 812, SE-98128 Kiruna, Sweden.

3 Observations and analysis

During the time period April 10-13, 1993, an attempt to detect X-ray radiation from Mars' atmosphere took place (G. S. Pankiewicz, Kent University, now at UK Meteorological Office). Three continuous observations were performed:

1. 1993-04-10, 01:24 - 01:45 UT
2. 1993-04-12, 16:54 - 17:29 UT
3. 1993-04-13, 23:27 - 23:45 UT

During observations nos. 1 and 3 the position of Mars was outside the central field of view of the telescope. During observation no. 2 Mars was expected to be located in the center of the field of view. Calculated positions of Mars are shown in Fig. 1 with arrows.

The above image and respective photon history files were found in the ROSAT archives. Since there is no visible object in the center of the image, it must be concluded that the result of the experiment was considered as negative. Here an attempt to analyze the photon history file in order to search for X-ray emission from the Martian atmosphere is presented. The purpose of the present search was to investigate whether there are any differences between the form of photon energy distribution at the expected position of Mars during observation no. 2 and at the same position during both reference observations.

The area examined in each image is rectangular, with pixel coordinates $5500 \leq X < 10500$ and $4000 \leq Y < 10000$, where X corresponds to R.A. and Y to declination. We use a square, sliding, window of size 400 by 400 pixels, that is moved in steps of 200 pixels, in the X and Y directions, covering the whole area. This results in a total of $n = 750$ window positions. At each window position we compute the average photon count in $m = 10$ energy channels. These channels are defined by linearly dividing the lowest 100 ROSAT PI channels into 10 bins. We then have an $m \times n$ matrix, y, of average photon counts. In order to decide whether there are distinct classes of vectors within the scanned area we use principal component analysis (PCA). The procedure has been performed for both: observation no. 2 and superimposed observations nos. 1 and 3. A PCA of the data matrix, y, is simply a change of basis,

$$y' = Ry,$$

where the rows of the orthogonal matrix R is the eigenvectors, r_j, of the covariance matrix of the original data points (the columns of y), ordered by the size of the corresponding eigenvalues. Row j in the matrix of new coordinates, y', corresponds to principal component j (PC_j). The magnitude of eigenvalue j can be interpreted as the amount of variance explained by PC_j. To view the contribution of PC_j in the original space we inverse transform by computing an $m \times n$ matrix, y'', whose columns are r_j, scaled by element (j, i) in y'. By averaging this matrix y'' over energy (along the columns) we get a vector, $\bar{y}''$, of length n. We can then view this vector as an image by associating each component with its original position in XY-coordinates.

4 Results

The three first (most significant) principal components were studied. A series of images: one pair for each PC, corresponding to the target observation and the reference observations, were created. The result is shown in Fig. 2. It is evident that Mars is visible close to the center of the image corresponding to the third PC, explaining only 10% of the total variance in photon energy distributions. PC_1 and PC_2 explain together 42% of the total variance. PC_3 of the reference observation does not show any signal in the center of the image, in spite of higher sensitivity used. The window positions responsible for the signal at the estimated position of Mars were identified and the corresponding original distributions of photons carefully analysed. A comparison of the average target distribution with the reference distribution is shown in Fig. 3.

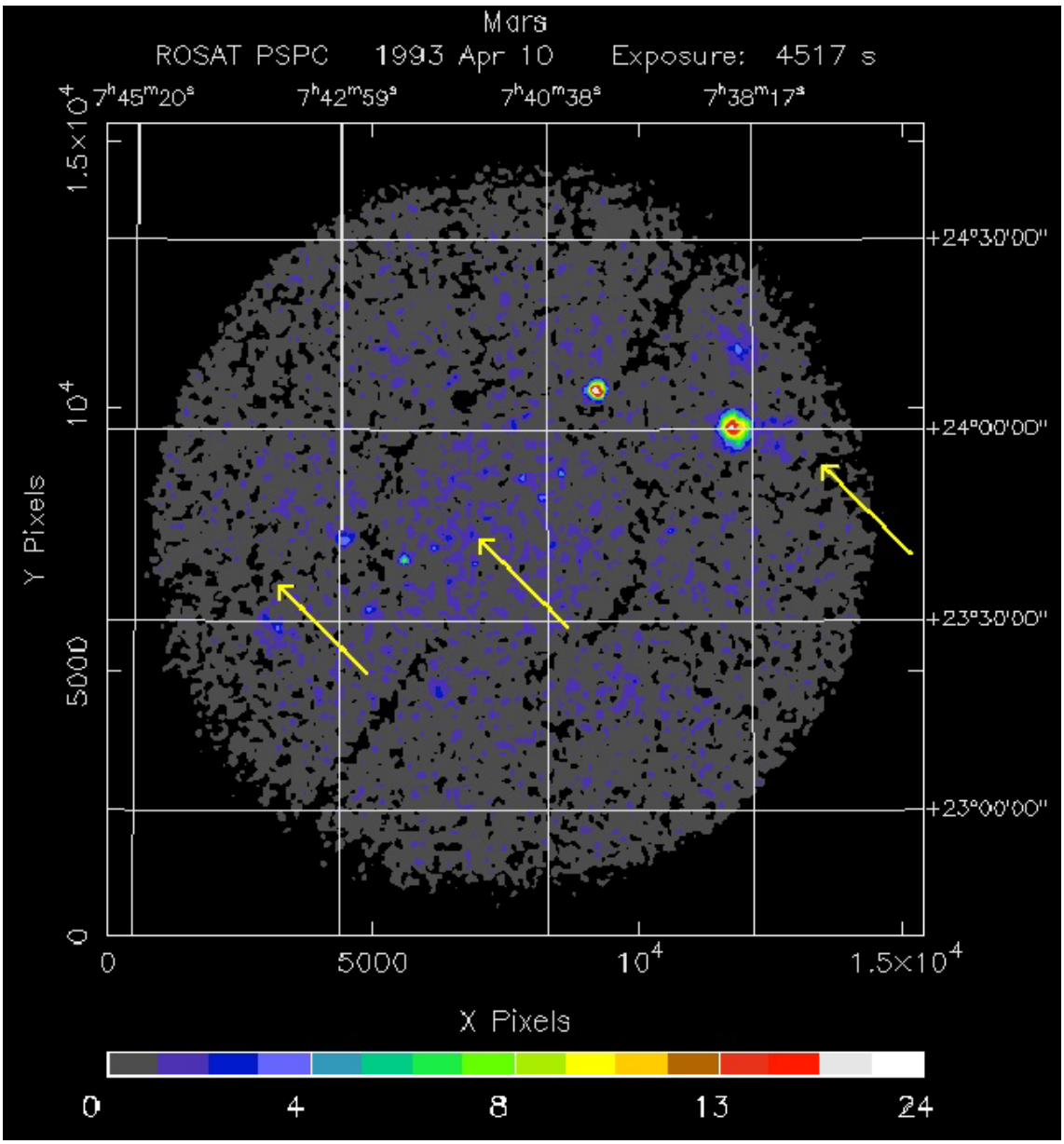

Figure 1: X-ray view of the portion of the sky where Mars was located on the dates of the observations. Arrows indicate the positions of Mars during the three observation periods.

Mars Reference observations

PC_1

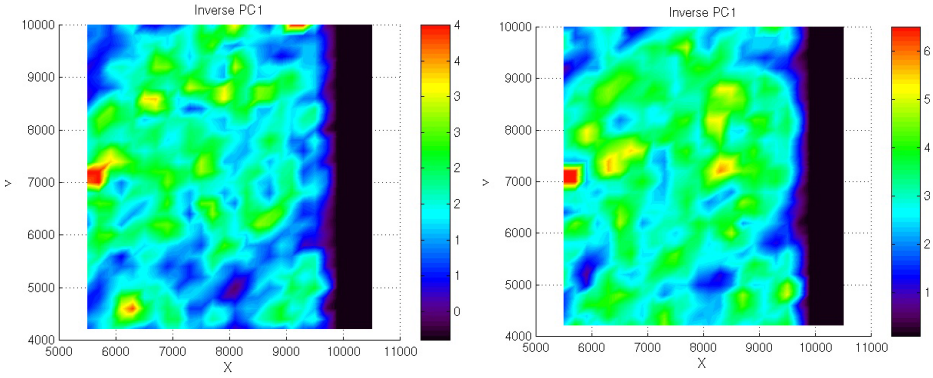

PC_2

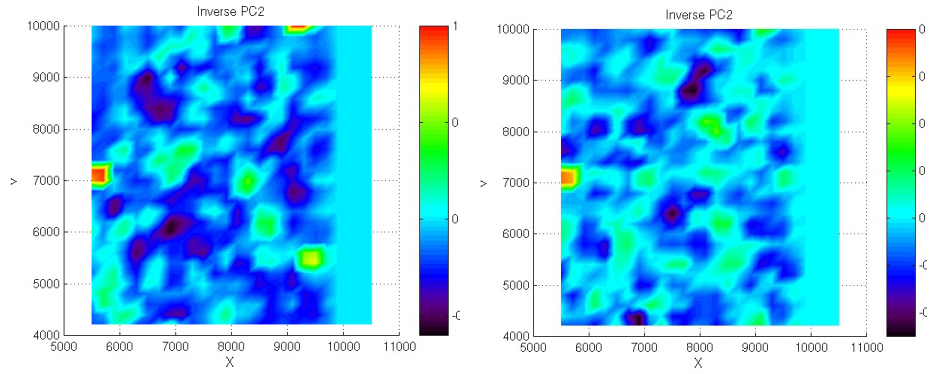

PC_3

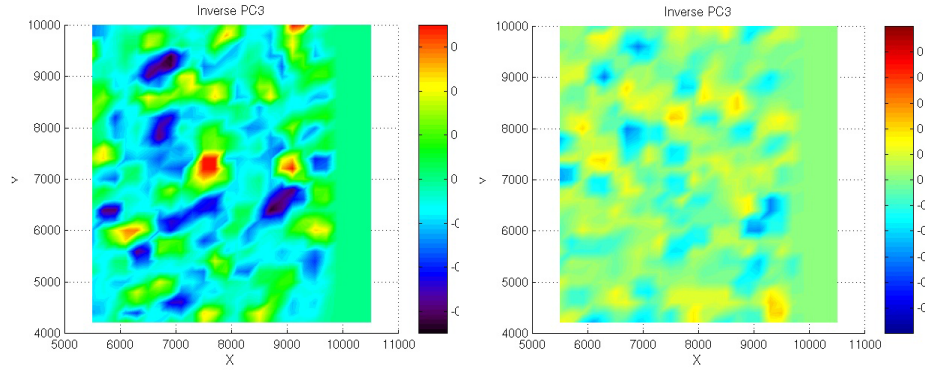

Figure 2: Composite images, constructed from average decomposed photon energy distributions: one pair for each PC, corresponding to: the target observation and, to the reference observations.

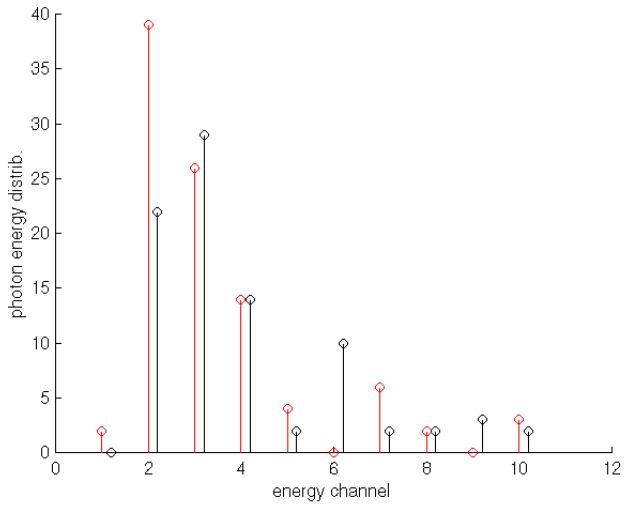

Figure 3: Photon energy distribution for the Mars image (black) together with that for the reference image (red). Channel 10 on the x-axis corresponds to 1 keV.

It may be seen that the difference between photon energy distributions is very small. Using a standard χ^2-test for two distributions it may be found that the difference between these two distributions is not significant. It is interesting to mention that if the distribution vectors are normalized to the maximum value within the vector, the signal maximum attributed here to Mars disappears. It means that the shape of the distribution does not contain enough information to discriminate the source. Both the absolute number of photons and the shape of distribution are needed to discriminate the source.

Considering that the averaged value of PC_3 for each window is expressed in photons/distribution bin, the total number of photons attributed to Mars ought to be 0.35×10 bins $= 3.5$ photons. Since there are at least two window positions containing these photons and since 0.75 of window area is redundant, the total number of photons that may be attributed to Mars could be between 4 and 7.

5 Conclusions

Soft X-ray emissions from Mars were found. The predicted count rate from simulations is an order of magnitude smaller than estimate derived using principal component analysis of the observed data. This can be a random deviation due to the low number of detected photons. Another possible explanations is the detection of photons emitted from outside the $6R_m \times 6R_m$ box of the simulated images.

References

[1] Cravens, T. E. 1997, Comet Hyakutake X-ray source: Charge transfer of solar wind heavy ions. *Geophys. Res. Lett.* **24**, 105-108.

[2] Holmström, M., S. Barabash and E. Kallio 2001, X-ray imaging of the solar wind—Mars interaction. In press, *Geophys. Res. Lett.*

[3] Lisse, C. M., K. Dennerl, J. Englhauser, M. Harden, F. E. Marshall, M. J. Mumma, R. Petre, J. P. Pye, M. J. Ricketts, J. Schmitt, J. Trümper and R. G. West 1996, Discovery of X-ray and extreme ultraviolet emission from comet C/Hyakutake 1996 B2. *Science* **274**, 205-209.